Inferring the Photolysis Rate of NO_2 in the Stratosphere Based on Satellite Observations

Jian Guan[1], Susan Solomon[1], Sasha Madronich[2,3], Douglas Kinnison[2]

[1]Department of Earth, Atmospheric, and Planetary Sciences, MIT; Cambridge, MA, 02139, USA

[2]Atmospheric Chemistry Observations and Modeling Laboratory, National Center for Atmospheric Research, Boulder, CO, 80301, USA

[3]USDA UV-B Monitoring and Research Program, Natural Resource Ecology Laboratory Colorado State University, Fort Collins, Colorado, 80523, USA

Correspondence to: Jian Guan (jianguan@mit.edu)

Abstract. NO and NO_2 (NO_x) play major roles in both tropospheric and stratospheric chemistry. This paper provides a novel method to obtain a global and accurate photodissociation coefficient for NO_2 based on satellite data. The photodissociation coefficient J_{NO_2} dominates the daytime diurnal variation of NOx photochemistry. Here the spatial variation of J_{NO_2} in 50° S-90° S in December from 20-40 km is obtained using data from the Michelson Interferometer for Passive Atmospheric Sounding (MIPAS) experiment. Because NO and NO_2 exchange rapidly with one another in the daytime, the J_{NO_2} can be attained assuming steady state, and the results are shown to be consistent with model results. The J_{NO_2} value decreases as the solar zenith angle increases and has a weak altitude dependence. A key finding is that the satellite-derived J_{NO_2} increases in the polar regions in good agreement with model predictions, due to the effects of ice and snow on surface albedo. Thus, the method presented here provides an observations-based check on the role of albedo in driving polar photochemistry.

1 Introduction

Fast photochemistry in the Earth's atmosphere is driven by sunlight and affects the diurnal variation of many species. The properties of sunlight entering the stratosphere, including light intensity and its energy distribution, depend on the solar zenith angle, as well as distributions of absorbing species. Further, the solar zenith angle is related to latitude, season, and local time. The sunlight entering the stratosphere determines the photochemical rates in the stratosphere, thus affecting stratospheric chemistry, and the diurnal variations of species concentration is one of the impacts. Therefore, diurnal variation observations provide key information in analyzing the photochemical properties of the stratosphere. NOx chemistry is one of the most important elements of stratospheric chemistry and plays a leading role in controlling stratospheric ozone concentration (Crutzen, 1979; Johnston, 1971; Crutzen, 1970). The photodissociation coefficient J_{NO_2} quantifies the process of NO_2 photolysis into NO, thus affecting the diurnal variation of NOx. The stratospheric NO and NO_2 abundances are controlled by the following reactions:

$$NO + O_3 \rightarrow NO_2 + O_2 \quad \text{(R1)}$$

$$NO_2 + h\nu \rightarrow NO + O \quad \text{(R2)}$$

$$NO_2 + O \rightarrow NO + O_2 \quad \text{(R3)}$$

$$ClO + NO \rightarrow NO_2 + Cl \quad \text{(R4)}$$

Because of the short lifetime of NO and NO_2, they are in steady state within the sunlit stratosphere. Therefore, the following equation holds:

$$\frac{[NO]}{[NO_2]} \approx \frac{J_{NO_2}+k_{O+NO_2}\times[O]}{(k_{NO+O_3}\times[O_3]+k_{NO+ClO}\times[ClO])} \quad (1)$$

A number of studies on the diurnal variation of NOx and J_{NO_2} in the stratosphere have been reported, based on models or airborne observations. Fabian et al. (1982) used a two-dimensional model to examine the diurnal variations of NOx at different altitudes. Many studies focused on the diurnal variation of NOx using airborne observations, and these were subsequently compared with models. (Pommereau, 1982; Roscoe et al., 1986; Kawa et al., 1990). Madronich et al. (1985) measured J_{NO_2} in the stratosphere utilizing a balloon platform and compared it to a model; they showed that the J_{NO_2} value has a weak altitude dependence. Webster and May (1987) measured the diurnal variation of NOx and J_{NO_2} simultaneously utilizing a balloon. Del Negro et al. (1999) calculated J_{NO_2} based on the concentrations of NO, NO_2, O_3, ClO, and HO_2 measured on an aircraft and BrO from a model, and compared them with a model. They found that the J_{NO_2} inferred from the data assuming steady state matched their model well. Moreover, it has been emphasized that albedo has a substantial effect on J_{NO_2} (Madronich, 1987; Bösch et al., 2001; Laepple, 2005; Walker et al., 2022). Further, the surface albedo over ice and snow has a large and important effect on tropospheric chemistry in the polar regions (Walker et al., 2022) due in large part to its effect on J_{NO_2}, highlighting the need to evaluate J_{NO_2} on a large scale. Surface radiometers have also been used to infer information about J_{NO_2} for different sky conditions in the troposphere (Shetter et al., 1992; Junkermann et al., 1989). However, aircraft, surface radiometers, or balloon measurements are all local and the amount of data is therefore limited. At the same time, models are based on theoretical calculations and require measured data for verification. These considerations are the motivation for this paper, in which satellite data are used to characterize J_{NO_2} on a global basis, with particular emphasis on values obtained over ice and snow.

Satellite measurements of NOx allow elucidation of its zenith angle and albedo dependence. The global concentrations of NO, NO_2, and related species as discussed below can be easily obtained using satellite data and used to determine J_{NO_2} at different latitudes, albedo, and altitudes. Solomon et al. (1986) reported satellite observations of the NO_2 diurnal variation in the stratosphere at solar zenith angles ranging from about 35 to 110 degrees but concurrent NO data were not available. Anderson et al. (1981) employed a similar method to study the zenith angle variation of mesospheric O_3. The Michelson Interferometer for Passive Atmospheric Sounding (MIPAS) is a Fourier transform spectrometer carried on Envisat, measuring not only NO_2 but also NO and O_3, as well as ClO, all of which are used here in inferring J_{NO_2} (see below). MIPAS was designed and operated for the measurement of atmospheric species from space and can detect limb emission in the middle atmosphere with high spectral resolution and low-noise performance (Fischer et al., 2008).

In this work, the novel method of obtaining the zenith angle dependence of NOx and J_{NO_2} using satellite data in summer over the polar cap is reported, taking 50° S-90° S in December in 20-40 km as an example. The diurnal variations of NOx and J_{NO_2} at different altitudes are described. J_{NO_2} changes with latitude are discussed and a J_{NO_2} map in the Antarctic is used to elucidate albedo effects. In summary, this work shows a method for obtaining NOx diurnal variation and accurate J_{NO_2} based on satellite data, expanding the way to attain information on this key photodissociation coefficient.

2 Data and Methods

2.1 MIPAS Data

The vertical resolution of MIPAS is approximately 3-8 km in the stratosphere, and the horizontal resolution is 30 km across track, about 500 km for along-track until 2004 (400 km after 2004). The vertical scan range is 5-150 km. Satellite operation was stopped temporarily in March 2004 due to technical issues and resumed in January 2005 in a new operation mode. MIPAS allows near complete global coverage, ranging from 87° S to 89° N obtained about every three days by 73 scans per orbit and 14.3 orbits per day. Each day the satellite passes through the same latitude at two local times (ascending side and descending side, as shown in

Fig. 1). Therefore, for this dataset, there are only two solar zenith angles at each latitude. We therefore focus on 50° S-90° S in the polar day, in December 2009, where there are as many solar zenith angles as possible in a relatively small latitude range. The data from the satellite was averaged daily and zonally (Because the specific latitudes of the satellite data vary somewhat from one orbit to another, we bin the data using a two-degree interval). Then we calculate the four-day running mean, which is shown in Fig. 2 and Fig. 3.

In this paper, we used the NO, NO_2, O_3, ClO, temperature and pressure data from V8 MIPAS retrievals performed with the IMK/IAA level 2 processor. The retrieval of temperature was reported by Kiefer et al. (2021). For NO retrieval, the method considered the populations of excited NO states (Funke et al., 2005). This implies that photolysis of NO_2 is included in the retrieval priors. However, retrieved NO is only weakly dependent on prior knowledge of J_{NO_2} values (10-15%). In our calculations, according to Eq. (2) and (3), NO, NO_2 and O_3 play comparable roles in calculation of J_{NO_2}, reducing the impact of prior knowledge on the final results. Therefore, prior knowledge of J_{NO_2} will have a small effect on our findings as long as prior knowledge of J_{NO_2} is not completely incorrect. The NO retrieval was documented by Funke et al. (2023). These authors reported an accuracy of 8-15% for altitudes of 20 to 40 km. Regarding O_3, Kiefer et al (2023) reported an accuracy of 3-8% in the altitude region of interest. The retrievals of NO_2 and ClO were described by Funke et al. (2005) and von Clarmann et al. (2009), respectively, with accuracies of 0.2-0.8 ppbv for NO_2 and total error of more than 35% for ClO. However, please note that these papers refer to older data versions. Accuracy estimates for V8 ClO and NO_2 are not yet available but the values quoted here were used as a rough guideline.

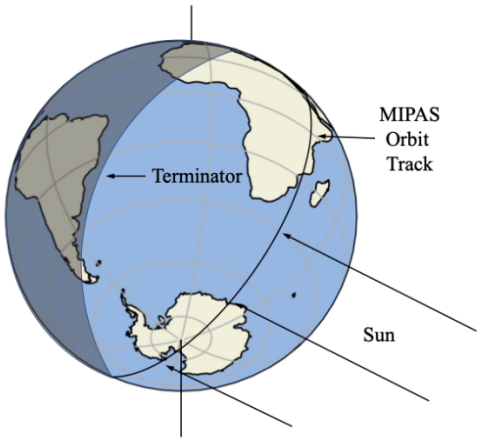

Figure 1. Schematic representation of the MIPAS orbit at high latitude in December showing the ascending (dayside) and descending (nightside) portions of the orbit and the terminator.

2.2 Model Calculations

The Whole Atmosphere Community Climate Model version 6 (WACCM6) is used in this study. WACCM6 is a component of the Community Earth System Model version 2 (CESM2; Gettelman et al., 2019; Danabasoglu et al., 2020). The horizontal resolution is 1.9° latitude × 2.5° longitude and the with 88 vertical levels up to about 140 km, with the altitude resolution increasing from 0.1 km near the surface to 1.0 km in the upper troposphere–lower stratosphere (UTLS) and 1–2 km in the stratosphere. This work uses the specified dynamics version of WACCM6, where the atmosphere below 50 km is nudged to the Modern-Era Retrospective Analysis for Research and Applications, version 2 (MERRA-2; Gelaro et al., 2017), temperature and wind fields with a relaxation time of 50 h. The chemistry mechanism includes a detailed representation of the middle atmosphere, with a sophisticated suite of gas-phase and heterogeneous chemistry reactions, including the Ox, NOx, HOx, ClOx, and BrOx reaction families. There are ~100 chemical species and ~300 chemical reactions. Reaction rates are updated following Jet Propulsion Laboratory (JPL) 2015

recommendations (Burkholder et al., 2015). The photolytic approach is based on both inline chemical modules (<200nm) and a lookup table approach (>200-750nm; see Kinnison et al., 2007). The look-up table (LUT) approach uses the Tropospheric Ultraviolet-Visible Radiation Model (TUV4.2; Madronich, 1987; Madronich and Weller, 1990), an advanced radiation transfer model widely used by the scientific community, using the four-stream pseudospherical discrete ordinates option. TUV has demonstrated excellent performance in intercomparisons with ground-based measurements, particularly under ideal sky conditions (Shetter et al., 2003). Model values for December 2009 at the same times and locations as the satellite data are selected by the satellite profile algorithm to compare with the satellite data, and denoted "Model". The satellite profile algorithm outputs constituents (e.g., J_{NO_2} and NOx concentrations) at the nearest latitude, longitude, and local time to the observation.

2.3 Chemical Equation

NO is assumed to be in a steady state in the sunlit atmosphere at 20-40 km at least for zenith angles less than 94°, due to its short lifetime. Using the chemistry discussed above, J_{NO_2} can then be expressed as

$$J_{NO_2} = \frac{[NO]}{[NO_2]} \times \left(k_{NO+O_3} \times [O_3] + k_{NO+ClO} \times [ClO]\right) - k_{O+NO_2} \times [O] \quad (2)$$

Where k is the rate constant, J_{NO_2} is the photodissociation coefficient of NO_2, and $[O_3]$ is the concentration of O_3.

To obtain the concentration of O, O is assumed to be in a steady state with ozone at 20-40 km. The concentration of O can be expressed as

$$[O] = \frac{J_{O_3} \times [O_3]}{k_{O+O_2+M} \times [O_2] \times [M]} \quad (3)$$

The k_{NO+O_3}, k_{NO+ClO}, k_{O+NO_2} and their uncertainties are from JPL (Burkholder et al., 2015), and k_{O+O_2+M} and its uncertainty are from International Union of Pure and Applied Chemistry (IUPAC; Atkinson et al., 2004). It is worth noting that J_{O_3} in the Eq. (3) comes from the model here, which is a limitation of this study. However, in the stratosphere below about 33 km [O] has a small effect on J_{NO_2}calculation (less than 8.1 percent) due to its low concentration (Johnston and Podolske, 1978). ClO can similarly be ignored when altitudes are less than 35 km, where ClO concentrations are small (Sagawa et al., 2013); otherwise using ClO data from MIPAS would introduce large and unnecessary uncertainty. HO_2 and BrO both can react with NO but they are not measured by MIPAS and their contributions to the partitioning between NO and NO_2 are negligibly small at the altitudes considered here (Del Negro et al., 1999). Therefore, we don't consider them in this paper.

3 Results and Discussion

3.1 NOx Concentration at different altitudes

To better understand the diurnal variation of NOx, concentrations of NO and NO_2 from MIPAS and the model are shown in Fig. 2 at different altitudes. The NO and NO_2 concentrations from MIPAS and the model show very good overall consistency. The solar zenith angle of 90 degrees is a clear dividing line, showing that light drives the diurnal variation, and the results are in good accord with the theory.

(a)

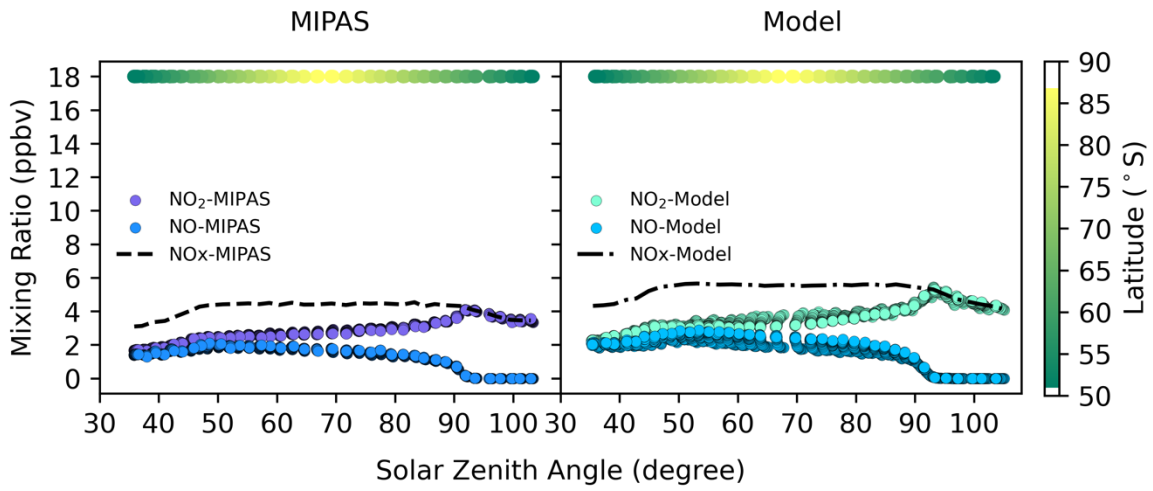

132

(b)

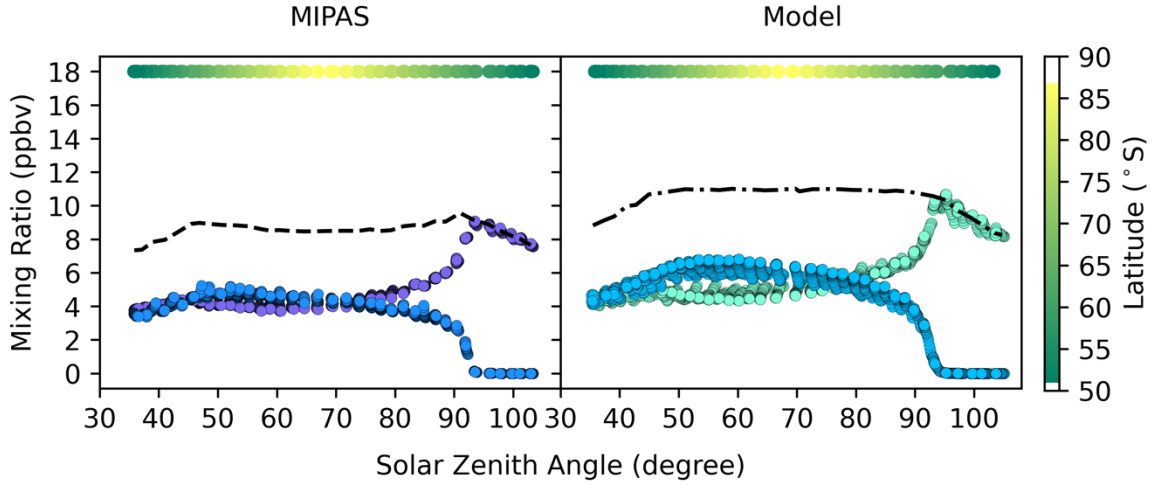

133

(c)

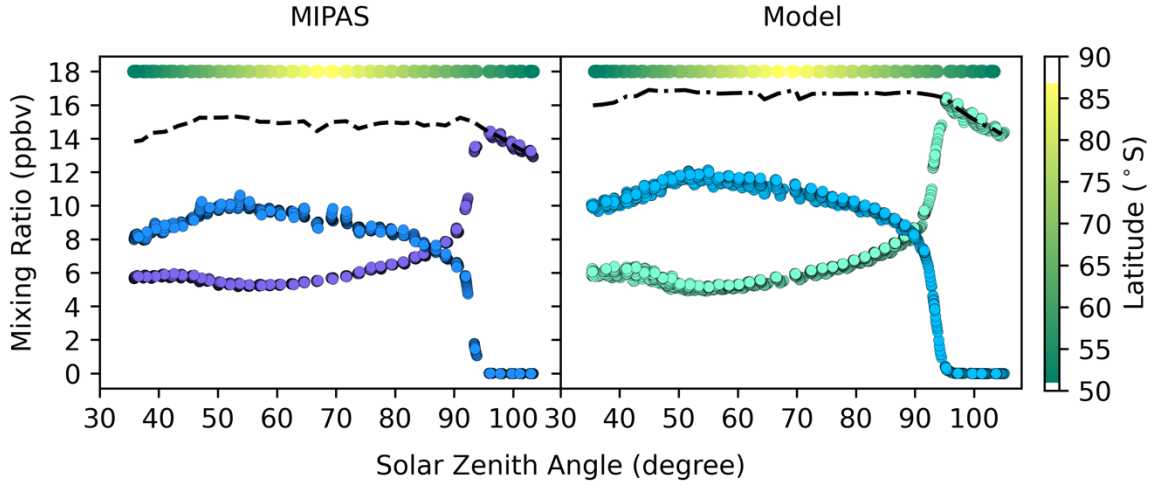

134

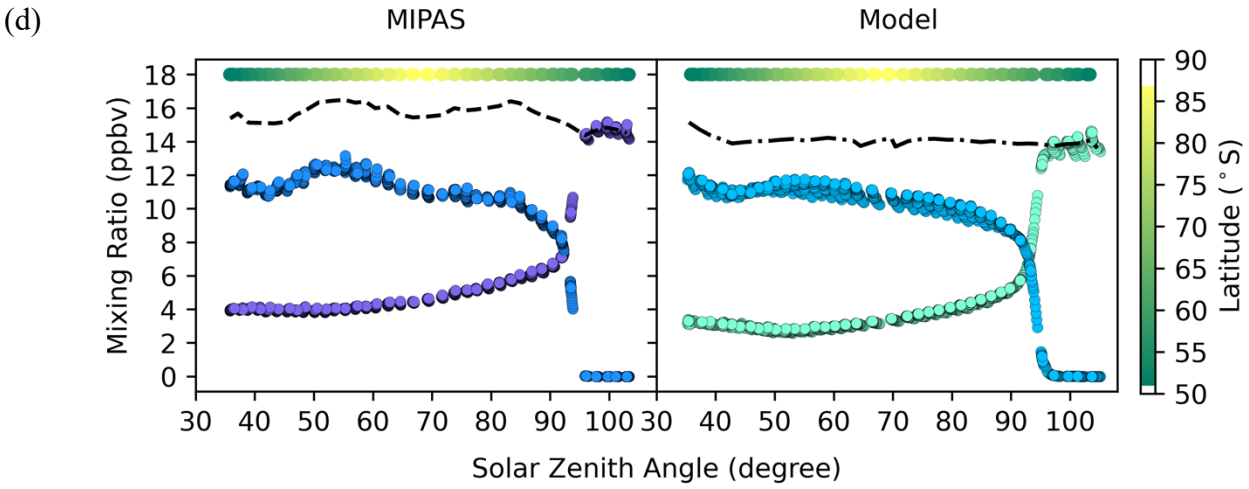

Figure 2. The concentrations of NO, NO_2 and NOx in 50° S-90° S in December 2009 from MIPAS and the model at different altitudes. (a) 23 km (b) 28 km (c) 33 km (d) 38km. Model values are at the same time and location as the satellite data. The color bar represents the latitude of the data points at each solar zenith angle. To ensure clear visual distinction for each point, black outlines are applied around them.

NO and NO_2 exchange with one another but their sum (NOx) varies relatively little for solar zenith angles less than about 90°. An increase in NO is matched by a decrease in NO_2 for zenith angles from about 30-50°, and then NO concentration decreases at larger angles, mainly reflecting changes in the photolysis rate as the satellite sweeps across the mid-latitudes and polar cap (see below). NO rapidly disappears when the solar zenith angle exceeds 90 degrees, and the concentrations of NO and NO_2 change dramatically during twilight. NO decreases rapidly while NO_2 increases rapidly. When the solar zenith angle is more than 90 degrees at these altitudes, NO is completely oxidized to NO_2, so there is no NO and NO_2/NOx is 1. In addition, the concentration of NO_2 decreases slightly when the solar zenith angle is more than 90 degrees, which indicates the formation of the N_2O_5.
It should also be noted that in Fig. 2, the concentrations of NO and NO_2 also reflect latitude variations, because the data at each zenith angle come from different latitudes as shown by the color bar at the top of each panel in Fig. 2, but these variations are fairly small over the summer polar cap and consistent with the model as shown. From 23 km to 33 km, the concentrations of NO and NO_2 increase with the altitude.

3.2 J_{NO_2} at different altitudes and solar zenith angles

Using Eq. (2) above, the J_{NO_2} and the error bar at different altitudes is shown in Fig. 3 along with the J_{NO_2} values from the model. The correlation diagrams show that the values inferred from the satellite observations are in excellent agreement with the model. Fig. 3 shows that the J_{NO_2} values at different altitudes within the 20-40 km range are nearly identical. This indicates the weak dependence of J_{NO_2} value on altitude, which was also reported by Madronich et al. (1985). This is because the NO_2 photolysis is largely driven by wavelengths ranging from 300 nm to 420nm (Madronich et al., 1983), which lie within a spectral region relatively free of atmospheric absorption. Consequently, the flux remains nearly constant at different altitudes. When the solar zenith angle is higher than about 90 degrees, the J_{NO_2} value drops rapidly to 0. The uncertainty is also shown in Fig. 3, and the model J_{NO_2} is within the error bar. The deviation between the results and model is significantly smaller than the 1-σ uncertainty, implying that the estimates of measurement errors of MIPAS may be conservative. To illustrate how different species affect our calculations at some altitudes, the effects of different gases at 38 km are shown in Fig. S1. The figure shows that O_3, O and ClO are critical to

NOx chemistry at 38 km. However, the concentrations of ClO and O are smaller at altitudes of less than 35 km, and have about 3.6% and less than 12% influence in our calculations, respectively. Moreover, the satellite data error of ClO becomes larger at lower altitudes, so ClO is not considered here when the altitude is lower than 35km.

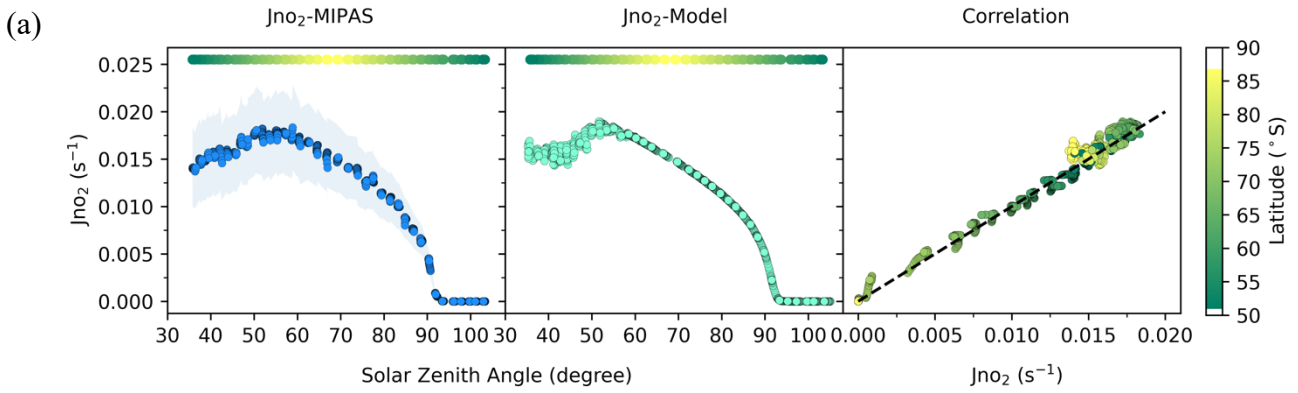

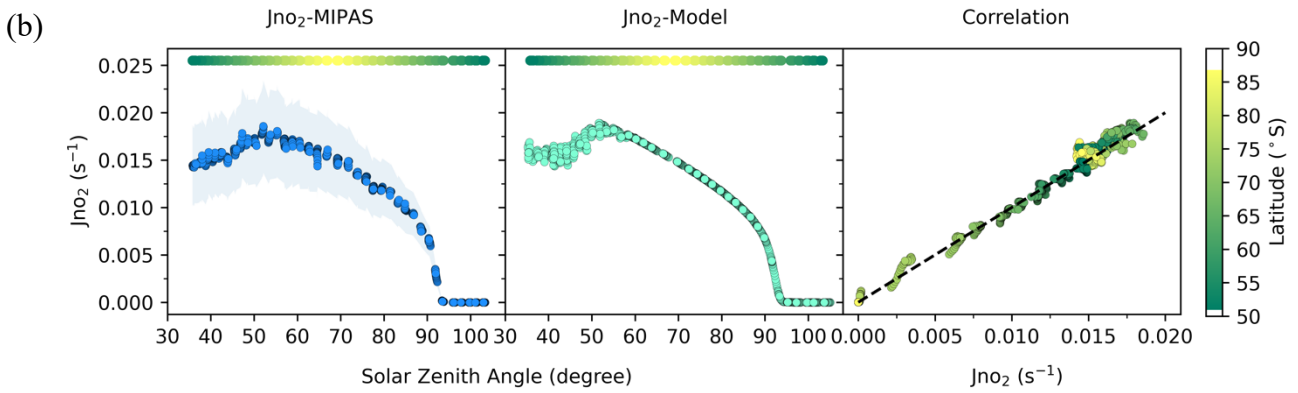

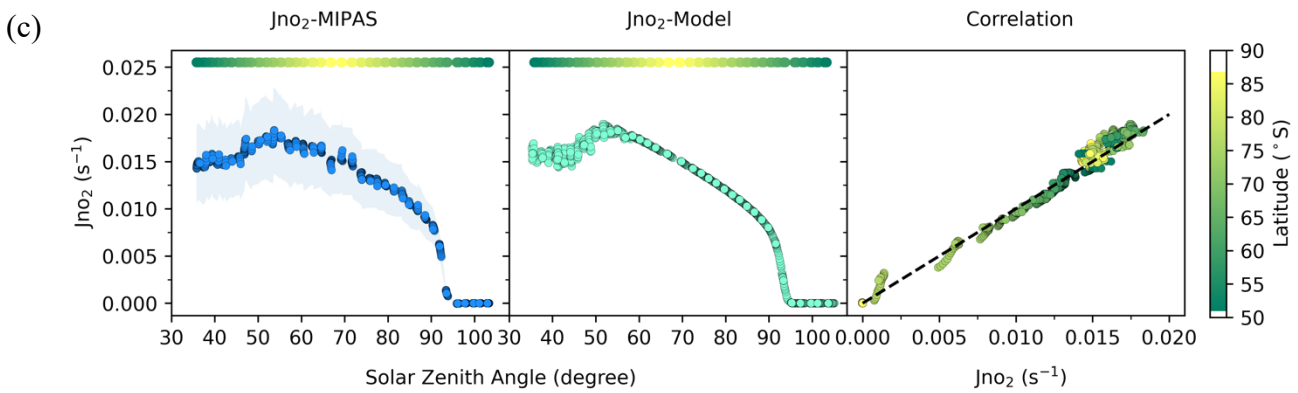

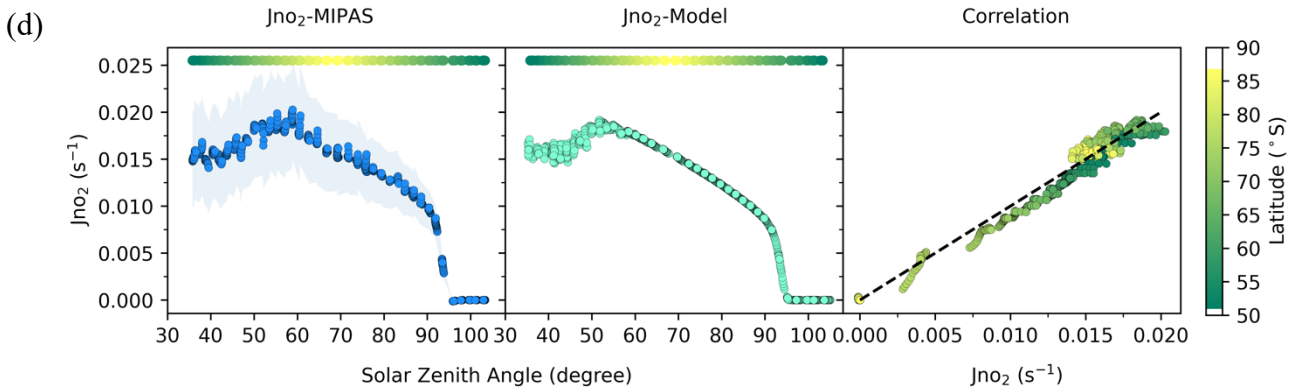

Figure 3. The J_{NO_2} in 50° S-90° S from MIPAS and the model at different altitudes. (a) 23 km (b) 28 km (c) 33 km (d) 38km. Model values are for the same time and location as the satellite data. The color bar represents the latitude of the data points at each solar zenith angle. In the correlation plots, the abscissa is J_{NO_2}-MIPAS and the ordinate is the J_{NO_2}-Model and the slope of dashed line is 1. To ensure clear visual distinction for each point, black outlines are applied around them.

3.3 J_{NO_2} at different latitudes

The J_{NO_2} values from the satellite and model at different latitudes are next discussed. The clear relationship between J_{NO_2} and latitude from MIPAS and model is also displayed in Fig. 4, and the close comparison between the two is remarkable. It is obvious that the satellite-inferred J_{NO_2} monotonically increases with latitude from 30° S-70° S, and then decreases at higher latitudes. The J_{NO_2} over the pole is taken at a larger solar zenith angle, which explains its decrease relative to surrounding parts of Antarctica. Fig. 5 displays maps of the detailed distributions of J_{NO_2} from MIPAS and model, which exhibits their excellent consistency and shows a sharp transition between mid-latitudes and the Antarctic continent or regions covered by sea ice.

The sharp transitions in J_{NO_2} values shown in Fig. 5 can only be caused by the large difference in albedo between the ocean and the Antarctic environs, covered by sea ice, land ice, and snow (Brandt et al., 2005; Shao and Ke, 2015). Albedo has a strong influence on J_{NO_2} because NO_2 is more sensitive than most atmospheric species to the effects of scattering and reflection (Madronich et al., 1983; Madronich, 1987; Bösch et al., 2001; Laepple et al., 2005). This is because the atmosphere exhibits considerable transparency at frequencies relevant to NO_2 photolysis, allowing a large number of photons to persist throughout the long atmospheric path, reaching Earth's surface and eventually returning to the stratosphere. In the high latitude area, the ground is covered with ice and snow, and the albedo can be as high as 0.9, while in the lower latitudes, the albedo is about 0.1 (Brandt et al., 2005; Shao and Ke, 2015). Table 1 shows the J_{NO_2} values at different solar zenith angles under different albedos. The results show that the albedo has a strong influence on the values, especially at low solar zenith angles. Based on Fig. 5, the J_{NO_2} above the continental ice is greater than that above the Antarctic sea ice, which may be because the fraction of open water within the pack influences the albedo (Brandt et al., 2005).

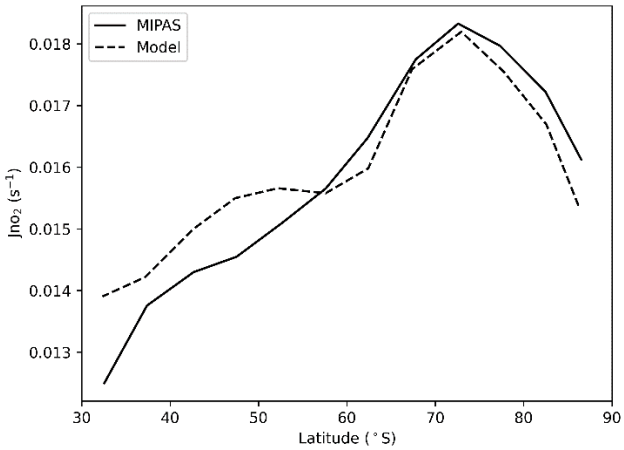

Figure 4. The relationship between J_{NO_2} and latitude from MIPAS and model in 30° S-90° S at 28 km. Model data is for the same time and location as the satellite data. J_{NO_2} is examined wherever the solar zenith angle is less than 70 degrees and averaged every five degrees of latitude.

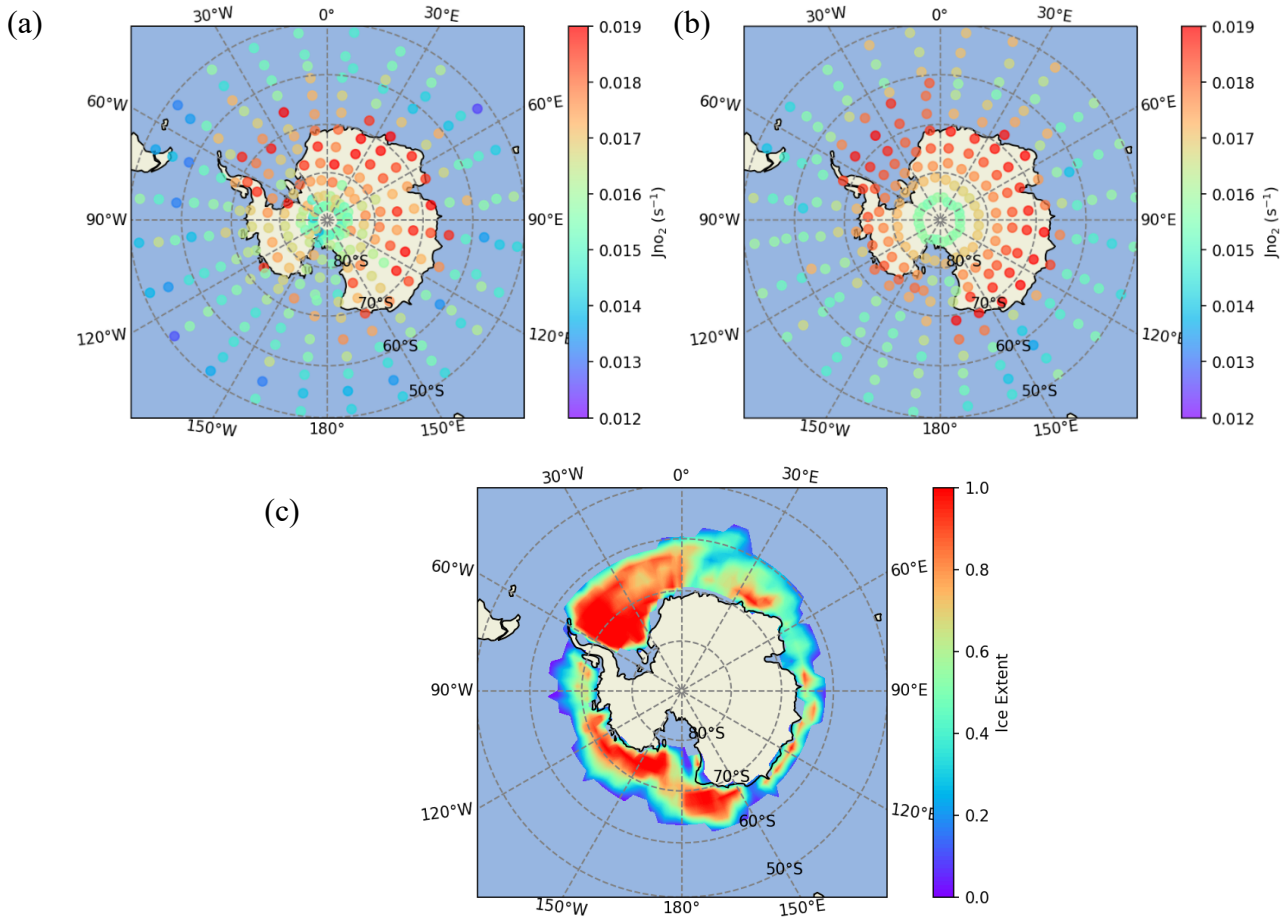

Figure 5. The mapping of J_{NO_2} in 50° S-90° S at 28 km from (a) MIPAS and (b) model. (c) The distribution of the sea ice extent in December 2009 in Antarctica from the model. Model J_{NO_2} data are for the same time and location as the satellite data. J_{NO_2} is shown wherever the solar zenith angle is less than 70 degrees and averaged every 3.33° latitude ×15° longitude.

Table 1. J_{NO_2} at different solar zenith angles under different albedos (α)

Solar zenith angle	J_{NO_2} ($\alpha = 0.1$)	J_{NO_2} ($\alpha = 0.9$)	J_{NO_2} ($\alpha = 0.9$)/J_{NO_2} ($\alpha = 0.1$)
0	1.30	2.21	1.70
10	1.30	2.19	1.69
20	1.29	2.14	1.65
30	1.28	2.05	1.59
40	1.27	1.92	1.52
50	1.24	1.77	1.42
60	1.20	1.58	1.31
70	1.14	1.36	1.20
80	1.01	1.10	1.09
90	0.664	0.673	1.01

4 Conclusions

The diurnal variations of NOx species and the resulting J_{NO_2} from about 50° S-90° S in December in 20-40 km have been evaluated based on MIPAS data. Light has a strong impact on the diurnal variations. NO and NO_2 are in steady state in the daytime and their sum is almost constant.

The calculated J_{NO_2} remarkably consistent with the model results, and the J_{NO_2} value decreases as the solar zenith angle increases. The J_{NO_2} value drops rapidly to 0 at the solar zenith angle of about 90 degrees. Moreover, the weak dependence of the J_{NO_2} value on altitude in this region is evident.

The results from the satellite and the model both indicate that J_{NO_2} increases with latitude, which can be attributed to more reflected light from ice and snow surfaces with high albedo. In summary, this work presents a new method for obtaining accurate J_{NO_2} values mainly based on satellite data. Further, this method can be extended to other photodissociation coefficients, paving the way for further tests of global photodissociation coefficients data based on satellites.

Code and data availability. The data and code are available at https://doi.org/10.5281/zenodo.7764756.

Supplement.

Author contributions. S.S. designed the study. J. G. analyzed the data and produced the figures. S. M. and D. K. run the models and contributed significantly to the interpretation of findings. J.G. wrote the manuscript, with comments from all authors.

Competing interests. The contact author has declared that none of the authors has any competing interests.

Disclaimer. Publisher's note: Copernicus Publications remains neutral with regard to jurisdictional claims in published maps and institutional affiliations.

Acknowledgements. Doug Kinnison was funded in part by NASA (grant no. 80NSSC19K0952). SS acknowledges support as the Martin Professor of environmental studies at MIT, while JG appreciates an MIT presidential fellowship. SM acknowledges partial support by the US Department of Agriculture (USDA) UV-B Monitoring and Research Program, Colorado State University, under USDA National Institute of Food and Agriculture Grant 2019-34263-30552; 2022-34263-38472. The CESM project is supported by the National Science Foundation and the Office of Science (BER) of the U.S. Department of Energy. We gratefully acknowledge high-performance computing support from Cheyenne (doi:10.5065/D6RX99HX) provided by NCAR's Computational and Information Systems Laboratory, sponsored by the National Science Foundation. We thank the Institute of Meteorology and Climate Research - Atmospheric Trace Gases and Remote Sensing, and Dr. Michael Kiefer and Dr. Gabriele Stiller for MIPAS data.

References

Anderson, G., Gille, J., Bailey, P., and Solomon, S.: LRIR observations of diurnal ozone variation in the mesosphere, Quadrennial International Ozone Symposium, 580–585, 1981.

Atkinson, R., Baulch, D. L., Cox, R. A., Crowley, J. N., Hampson, R. F., Hynes, R. G., Jenkin, M. E., Rossi, M. J., and Troe, J.: Evaluated kinetic and photochemical data for atmospheric chemistry: Volume I - gas phase reactions of Ox, HOx, NOx and SOx species, Atmos. Chem. Phys., 4, 1461–1738, https://doi.org/10.5194/acp-4-1461-2004, 2004.

Bösch, H., Camy-Peyret, C., Chipperfield, M., Fitzenberger, R., Harder, H., Schiller, C., Schneider, M., Trautmann, T., and Pfeilsticker, K.: Comparison of measured and modeled stratospheric UV/Visible actinic fluxes at large solar zenith angles, Geophys. Res. Lett., 28, 1179–1182, https://doi.org/10.1029/2000GL012134, 2001.

Brandt, R. E., Warren, S. G., Worby, A. P., and Grenfell, T. C.: Surface Albedo of the Antarctic Sea Ice Zone, J. Climate, 18, 3606–3622, https://doi.org/10.1175/JCLI3489.1, 2005.

Burkholder, J. B., Sander, S. P., Abbatt, J. P. D., Barker, J. R., Huie, R. E., Kolb, C. E., Kurylo, M. J., Orkin, V. L., Wilmouth, D. M., and Wine, P. H.: Chemical kinetics and photochemical data for use in atmospheric studies: evaluation number 18, Pasadena, CA: Jet Propulsion Laboratory, National Aeronautics and Space Administration, 2015.

Crutzen, P. J.: The influence of nitrogen oxides on the atmospheric ozone content, Quarterly Journal of the Royal Meteorological Society, 96, 320–325, https://doi.org/10.1002/qj.49709640815, 1970.

Crutzen, P. J.: The Role of NO and NO_2 in the Chemistry of the Troposphere and Stratosphere, Annu. Rev. Earth Planet. Sci., 7, 443–472, https://doi.org/10.1146/annurev.ea.07.050179.002303, 1979.

Danabasoglu, G., Lamarque, J. -F., Bacmeister, J., Bailey, D. A., DuVivier, A. K., Edwards, J., Emmons, L. K., Fasullo, J., Garcia, R., Gettelman, A., Hannay, C., Holland, M. M., Large, W. G., Lauritzen, P. H., Lawrence, D. M., Lenaerts, J. T. M., Lindsay, K., Lipscomb, W. H., Mills, M. J., Neale, R., Oleson, K. W., Otto-Bliesner, B., Phillips, A. S., Sacks, W., Tilmes, S., Kampenhout, L., Vertenstein, M., Bertini, A., Dennis, J., Deser, C., Fischer, C., Fox-Kemper, B., Kay, J. E., Kinnison, D., Kushner, P. J., Larson, V. E., Long, M. C., Mickelson, S., Moore, J. K., Nienhouse, E., Polvani, L., Rasch, P. J., and Strand, W. G.: The Community Earth System Model Version 2 (CESM2), J. Adv. Model. Earth Syst., 12, https://doi.org/10.1029/2019MS001916, 2020.

Del Negro, L. A., Fahey, D. W., Gao, R. S., Donnelly, S. G., Keim, E. R., Neuman, J. A., Cohen, R. C., Perkins, K. K., Koch, L. C., Salawitch, R. J., Lloyd, S. A., Proffitt, M. H., Margitan, J. J., Stimpfle, R. M., Bonne, G. P., Voss, P. B., Wennberg, P. O., McElroy, C. T., Swartz, W. H., Kusterer, T. L., Anderson, D. E., Lait, L. R., and Bui, T. P.: Comparison of modeled and observed values of NO_2 and JNO_2 during the Photochemistry of Ozone Loss in the Arctic Region in Summer (POLARIS) mission, J. Geophys. Res., 104, 26687–26703, https://doi.org/10.1029/1999JD900246, 1999.

Fabian, P., Pyle, J. A., and Wells, R. J.: Diurnal variations of minor constituents in the stratosphere modeled as a function of latitude and season, J. Geophys. Res., 87, 4981, https://doi.org/10.1029/JC087iC07p04981, 1982.

Fischer, H., Birk, M., Blom, C., Carli, B., Carlotti, M., Endemann, M., Flaud, J. M., Gessner, R., Kleinert, A., Koopman, R., Langen, J., Lopez-Puertas, M., Mosner, P., Nett, H., Oelhaf, H., Perron, G., Remedios, J., Ridolfi, M., Stiller, G., and Zander, R.: MIPAS: an instrument for atmospheric and climate research, Atmos. Chem. Phys., https://doi.org/10.5194/acp-8-2151-2008, 2008.

Funke, B., López-Puertas, M., von Clarmann, T., Stiller, G. P., Fischer, H., Glatthor, N., Grabowski, U., Höpfner, M., Kellmann, S., Kiefer, M., Linden, A., Mengistu Tsidu, G., Milz, M., Steck, T., and Wang, D. Y.: Retrieval of stratospheric NOx from 5.3 and 6.2 μm nonlocal thermodynamic equilibrium emissions measured by Michelson Interferometer for Passive Atmospheric Sounding (MIPAS) on Envisat, Journal of Geophysical Research: Atmospheres, 110, https://doi.org/10.1029/2004JD005225, 2005.

Funke, B., García-Comas, M., Glatthor, N., Grabowski, U., Kellmann, S., Kiefer, M., Linden, A., López-Puertas, M., Stiller, G. P., and von Clarmann, T.: Michelson Interferometer for Passive Atmospheric Sounding Institute of Meteorology and Climate Research/Instituto de Astrofísica de Andalucía version 8 retrieval of nitric oxide and lower-thermospheric temperature, Atmos. Meas. Tech., 16, 2167–2196, https://doi.org/10.5194/amt-16-2167-2023, 2023.

Gelaro, R., McCarty, W., Suárez, M. J., Todling, R., Molod, A., Takacs, L., Randles, C. A., Darmenov, A., Bosilovich, M. G., Reichle, R., Wargan, K., Coy, L., Cullather, R., Draper, C., Akella, S., Buchard, V., Conaty, A., da Silva, A. M., Gu, W., Kim, G.-K., Koster, R., Lucchesi, R., Merkova, D., Nielsen, J. E., Partyka, G., Pawson, S., Putman, W., Rienecker, M., Schubert, S. D., Sienkiewicz, M., and Zhao, B.: The Modern-Era Retrospective Analysis for Research and Applications, Version 2 (MERRA-2), J. Climate, 30, 5419–5454, https://doi.org/10.1175/JCLI-D-16-0758.1, 2017.

Gettelman, A., Mills, M. J., Kinnison, D. E., Garcia, R. R., Smith, A. K., Marsh, D. R., Tilmes, S., Vitt, F., Bardeen, C. G., McInerny, J., Liu, H. -L., Solomon, S. C., Polvani, L. M., Emmons, L. K., Lamarque, J. -F., Richter, J. H., Glanville, A. S., Bacmeister, J. T., Phillips, A. S., Neale, R. B., Simpson, I. R., DuVivier, A. K., Hodzic, A., and Randel, W. J.: The Whole Atmosphere Community Climate Model Version 6 (WACCM6), JGR Atmos., 124, 12380–12403, https://doi.org/10.1029/2019JD030943, 2019.

Johnston, H.: Reduction of Stratospheric Ozone by Nitrogen Oxide Catalysts from Supersonic Transport Exhaust, Science, 173, 517–522, https://doi.org/10.1126/science.173.3996.517, 1971.

Johnston, H. S. and Podolske, J.: Interpretations of stratospheric photochemistry, Rev. Geophys., 16, 491–519, https://doi.org/10.1029/RG016i004p00491, 1978.

Junkermann, W., Platt, U., and Volz-Thomas, A.: A photoelectric detector for the measurement of photolysis frequencies of ozone and other atmospheric molecules, J. Atmos. Chem., 8, 203–227, https://doi.org/10.1007/BF00051494, 1989.

Kawa, S. R., Fahey, D. W., Solomon, S., Brune, W. H., Proffitt, M. H., Toohey, D. W., Anderson, D. E., Anderson, L. C., and Chan, K. R.: Interpretation of aircraft measurements of NO, ClO, and O_3 in the lower stratosphere, J. Geophys. Res., 95, 18597, https://doi.org/10.1029/JD095iD11p18597, 1990.

Kiefer, M., von Clarmann, T., Funke, B., García-Comas, M., Glatthor, N., Grabowski, U., Kellmann, S., Kleinert, A., Laeng, A., Linden, A., López-Puertas, M., Marsh, D. R., and Stiller, G. P.: IMK/IAA MIPAS temperature retrieval version 8: nominal measurements, Atmos. Meas. Tech., 14, 4111–4138, https://doi.org/10.5194/amt-14-4111-2021, 2021.

Kiefer, M., von Clarmann, T., Funke, B., García-Comas, M., Glatthor, N., Grabowski, U., Höpfner, M., Kellmann, S., Laeng, A., Linden, A., López-Puertas, M., and Stiller, G. P.: Version 8 IMK–IAA MIPAS ozone profiles: nominal observation mode, Atmos. Meas. Tech., 16, 1443–1460, https://doi.org/10.5194/amt-16-1443-2023, 2023.

Kinnison, D. E., Brasseur, G. P., Walters, S., Garcia, R. R., Marsh, D. R., Sassi, F., Harvey, V. L., Randall, C. E., Emmons, L., Lamarque, J. F., Hess, P., Orlando, J. J., Tie, X. X., Randel, W., Pan, L. L., Gettelman, A., Granier, C., Diehl, T., Niemeier, U., and Simmons, A. J.: Sensitivity of chemical tracers to meteorological parameters in the MOZART-3 chemical transport model, J. Geophys. Res., 112, D20302, https://doi.org/10.1029/2006JD007879, 2007.

Laepple, T., Schultz, M. G., Lamarque, J. F., Madronich, S., Shetter, R. E., Lefer, B. L., and Atlas, E.: Improved albedo formulation for chemistry transport models based on satellite observations and assimilated snow data and its impact on tropospheric photochemistry, J. Geophys. Res., 110, D11308, https://doi.org/10.1029/2004JD005463, 2005.

Madronich, S.: Photodissociation in the atmosphere: 1. Actinic flux and the effects of ground reflections and clouds, J. Geophys. Res., 92, 9740, https://doi.org/10.1029/JD092iD08p09740, 1987.

Madronich, S. and Weller, G.: Numerical integration errors in calculated tropospheric photodissociation rate coefficients, J Atmos Chem, 10, 289–300, https://doi.org/10.1007/BF00053864, 1990.

Madronich, S., Hastie, D. R., Ridley, B. A., and Schiff, H. I.: Measurement of the photodissociation coefficient of NO_2 in the atmosphere: I. Method and surface measurements, J. Atmos. Chem., 1, 3–25, https://doi.org/10.1007/BF00113977, 1983.

Madronich, S., Hastie, D. R., Schiff, H. I., and Ridley, B. A.: Measurement of the photodissociation coefficient of NO2 in the atmosphere: II, stratospheric measurements, J. Atmos. Chem., 3, 233–245, https://doi.org/10.1007/BF00210498, 1985.

Pommereau, J. P.: Observation of NO_2 diurnal variation in the stratosphere, Geophys. Res. Lett., 9, 850–853, https://doi.org/10.1029/GL009i008p00850, 1982.

Roscoe, H. K., Kerridge, B. J., Gray, L. J., Wells, R. J., and Pyle, J. A.: Simultaneous measurements of stratospheric NO and NO_2 and their comparison with model predictions, J. Geophys. Res., 91, 5405, https://doi.org/10.1029/JD091iD05p05405, 1986.

Sagawa, H., Sato, T. O., Baron, P., Dupuy, E., Livesey, N., Urban, J., Von Clarmann, T., De Lange, A., Wetzel, G., Connor, B. J., Kagawa, A., Murtagh, D., and Kasai, Y.: Comparison of SMILES ClO profiles with satellite, balloon-borne and ground-based measurements, Atmos. Meas. Tech., 6, 3325–3347, https://doi.org/10.5194/amt-6-3325-2013, 2013.

Shao, Z.-D. and Ke, C.-Q.: Spring–summer albedo variations of Antarctic sea ice from 1982 to 2009, Environ. Res. Lett., 10, 064001, https://doi.org/10.1088/1748-9326/10/6/064001, 2015.

Shetter, R., Junkermann, W., Swartz, W., Frost, G., Crawford, J., Lefer, B., Barrick, J., Hall, S., Hofzumahaus, A., Bais, A., Calvert, J. G., Cantrell, C. A., Madronich, S., muller, M., Kraus, A., Monks, P. S., Edwards, G. D., McKenzie, R., Johnston, P., Schmitt, R., Griffioen, E., Krol, M., Kylling, A., Dickerson, R. R., Lloyd, S. A., Martin, T., Gardiner, B., Mayer, B., Pfister, E., Roth, E. P., keopke, P., Ruggaber, A., Schwander, H., and van Weele, M.: Photolysis frequency of NO 2: measurement and modeling during the International Photolysis Frequency Measurement and Modeling Intercomparison (IPMMI), J. Geophys. Res.: Atmos., 108, 2003.

Shetter, R. E., McDaniel, A. H., Cantrell, C. A., Madronich, S., and Calvert, J. G.: Actinometer and Eppley radiometer measurements of the NO $_2$ photolysis rate coefficient during the Mauna Loa Observatory photochemistry experiment, J. Geophys. Res., 97, 10349, https://doi.org/10.1029/91JD02289, 1992.

Solomon, S., Russell, J. M., and Gordley, L. L.: Observations of the diurnal variation of nitrogen dioxide in the stratosphere, J. Geophys. Res., 91, 5455, https://doi.org/10.1029/JD091iD05p05455, 1986.

Von Clarmann, T., Höpfner, M., Kellmann, S., Linden, A., Chauhan, S., Funke, B., Grabowski, U., Glatthor, N., Kiefer, M., and Schieferdecker, T.: Retrieval of temperature, H_2O, O_3, HNO_3, CH_4, N_2O, $ClONO_2$ and ClO from MIPAS reduced resolution nominal mode limb emission measurements, Atmospheric Measurement Techniques, 2, 159–175, https://doi.org/10.5194/amt-2-159-2009, 2009.

Webster, C. R. and May, R. D.: Simultaneous in situ measurements and diurnal variations of NO, NO_2, O_3, j NO_2, CH_4, H_2O, and CO_2 in the 40- to 26-km region using an open path tunable diode laser spectrometer, J. Geophys. Res., 92, 11931, https://doi.org/10.1029/JD092iD10p11931, 1987.